


FULL PAPER

Open Access



# Global and local Joule heating during substorms in St. Patrick's Day 2015 geomagnetic storm

K. J. Suji and P. R. Prince\* 

## Abstract

The first super storm of solar cycle 24 occurred on "St. Patrick's Day" (17 March 2015), with a minimum Dst level of  $-223$  nT. Five major substorms in this super storm were selected, with minimum values of local electrojet index (IL) ranging from  $-1662$  to  $-673$  nT. The selected substorms are all in the 22:00 MLT–06:00 MLT sector of the auroral oval region showing associated Pi2s and negative bays in the H-component of magnetograms, derived from the IMAGE magnetometer longitudinal (Fennoscandia) chain. The solar wind energy input is estimated as time integral of Akasofu's epsilon parameter, determined from the SuperMAG magnetometer. The local ionospheric Joule heating (local JH) rate, in the midnight or post-midnight sectors, is estimated using a modified form of Ahn's empirical conversion. The Global ionospheric Joule heating rate in the northern hemisphere (global JH) is taken from OpenGGCM model. For the substorm in the main phase of the superstorm, the local JH consumes only 9% (8%, if the IL is replaced by AL index in the empirical conversion relation) of the global JH. However, 40–86% (39–48%, if the IL is replaced by AL index in the empirical conversion relation) of global JH is consumed as local JH for the remaining substorms.

**Keywords:** Geomagnetic storms, Substorms, Pi2 pulsations, Ionospheric Joule heating

## Introduction

Ionospheric Joule heating (JH), the dominant solar wind energy dissipation mainly in the E region of earth's ionosphere, depends on injection of energetic particle fluxes into the auroral oval region during magnetospheric substorms, due to kinetic instability, that occurs in the mid-tail magnetic lobes. The precipitated particle fluxes then collide with neutrals and lose their kinetic energy in the form of Joule heating. Since this precipitation is more localised in the auroral oval region, the heat generated is highly concentrated around this region as well.

When considering isolated substorms, solar wind energy dissipated in the auroral ionosphere has the contribution of substorms only, whereas the solar wind energy dissipated in the auroral ionosphere has contribution of both storms and substorms during substorms associated with a geomagnetic storm. The total

dissipation, in this case, can be found out by considering the geomagnetic storms and the associated substorms as distinct phenomena. It is found recently that Joule heating generated during geomagnetic storms is more concentrated in cusp region of the auroral ionosphere, whereas that during substorms is more focused in the auroral oval region of the auroral ionosphere (Palmroth et al. 2004a). Also, it had been confirmed over a few decades that magnetospheric substorms frequently occur in the midnight sector of the auroral oval region since energetic electron flux bursts out directly from mid-tail lobes.

Spatial asymmetry of JH in different sectors of auroral oval has been studied by several authors (Xiong et al. 2014; Foster et al. 1983; Palmroth et al. 2004a; Brekke and Rino 1978; Vickrey et al. 1982). According to Palmroth et al. (2004a), JH asymmetries were attributed to localised current closure near the surges of substorm current wedge. Foster et al. (1983) argued that midnight sector heating is more pronounced during intense substorms. This enhancement is mainly due to intense electric field

\*Correspondence: princerprasad@gmail.com  
Department of Physics, University College, Thiruvananthapuram, Kerala 695034, India

and more particle precipitations during auroral substorms. McHarg et al. (2005) have discussed JH asymmetries over pre-midnight and post-midnight sectors of the auroral oval. They found that spatial asymmetry is due to the difference in electron flux precipitations at these sectors under strongly southward IMF. Because of these asymmetries in Joule heating in the auroral oval, a global proxy is not well suited for analysing the local response of ionospheric Joule heating (local JH).

Global JH during storm-time substorms has been studied critically for the first time by Ahn et al. (1983). They estimated the global contribution of JH using specifically designed numerical simulation techniques, with advanced version of the AL index derived from 71 magnetometer stations around auroral oval region. In subsequent studies using different MHD simulation techniques, global JH has been carefully addressed (Lu et al. 1998; Knipp et al. 1998; Richmond 1992; Slinker et al. 1999; Palmroth et al. 2004a, b, 2005). However, studies of global dissipation of JH during substorms using global indices deduced from the observations of limited numbers of stations, and of global dissipation of JH estimated using a single meridional magnetometer chain are questionable. Meanwhile, local JH in a typical sector of the auroral oval is conceptually strong, as far as the substorm in midnight sector of the auroral oval is concerned. However, comparison of local JH, which was localised around magnetospheric onset locations, with global JH, generated over auroral ionosphere during storm-time substorms, has not been addressed extensively.

The present paper discusses the global as well as the local perspective of Joule heating during magnetospheric

substorms associated with the St. Patrick's Day geomagnetic storm on March 17, 2015. In the present study, five major substorms over the course of St. Patrick's Day geomagnetic storm (first super storm in SC 24) are used for this purpose. The study focuses on the significance of Joule heating associated with substorms in night side auroral sector (22:00 MLT–06:00 MLT). Pi2s derived from H-component of magnetic disturbances, observed in the IMAGE magnetometer longitudinal (Fennoscandia) chain, are used as identifiers of these substorms.

### Data and methodology

Solar wind and IMF data are taken from the WIND Spacecraft located at  $\sim 200 R_E$  on the Sun–Earth line (L1 point). The 10 s resolution local index (IL) is estimated from north–south magnetic disturbances observed in the IMAGE array of ground magnetometers (<http://space.fmi.fi/image/beta/>) (Tanskanen 2009). The base level for a day is defined as the quietest period of 15–60 min. If the day is geomagnetically active, with  $Dst < -50$  nT, then the base level is determined from quietest periods of the previous or the following day. The lower envelope of the superposed X-component of the magnetic disturbances observed in each station after subtracting the base level gives the IL index, with a resolution of 10 s. Measurements from Fennoscandia magnetometer chain (Table 1), which includes 22 high-latitude magnetometer stations covering auroral oval region at midnight or post-midnight sectors, are used. The H-components of magnetic disturbances at each station are derived using the expression,  $\sqrt{X^2 + Y^2}$  where  $X$  is the field vector of magnetic disturbance along geographic north and  $Y$  is the field

**Table 1** List of selected ground magnetometer stations in the IMAGE magnetometer network and their geographic and corrected coordinates

No.	Name	Code	Geogr. latitude (°)	Geogr. longitude (°)	CGM latitude (°)	CGM longitude (°)
1	Abisko	ABK	68.35	18.82	65.3	101.75
2	Andenes	AND	69.3	16.03	66.45	100.37
3	Ivalo	IVA	68.56	27.29	65.1	108.57
4	Kevo	KEV	69.76	27.01	66.32	109.24
5	Kilpisjärvi	KIL	69.06	20.77	65.94	103.8
6	Kiruna	KIR	67.84	20.42	64.69	102.64
7	Lycksele	LYC	64.61	18.75	61.44	99.29
8	Masi	MAS	69.46	23.7	66.18	106.42
9	Mekrijärvi	MEK	62.77	30.97	59.1	108.45
10	Oulujärvi	OUJ	64.52	27.23	60.99	106.14
11	Pello	PEL	66.9	24.08	63.55	104.92
12	Rørvik	RVK	64.94	10.98	62.23	93.31
13	Sodankylä	SOD	67.37	26.63	63.92	107.26
14	Tromsø	TRO	69.66	18.94	66.64	102.9

vector of magnetic disturbance along geographic east directions.

For identifying high-latitude Pi2 events, 10-s resolution data from IMAGE magnetometer network located in high latitude was used. The Pi2 events are identified from band-pass filtered (6–25 mHz) time series of H-components observed at each station. For band-pass filtering, Butterworth band-pass filter of order 4 with cutoff frequencies 6 mHz and 25 mHz was used (Kozlovskaya and Kozlovsky 2012; Behera et al. 2017). The time series, thus obtained, showed a sudden impulse in the frequency range 6.6–25 mHz, which is marked as associated Pi2 events. To confirm its association with substorm activity, AL and Wp indices were further selected and analysed. The AL, Wp and Dst indices are taken from World Data Center (WDC), Kyoto (<http://wdc.kugi.kyoto-u.ac.jp/>).

The solar wind energy transfer into the MI system mainly depends on dynamo action (Akasofu 1981) between solar wind and the Earth's magnetosphere. To determine solar wind energy input, numerous coupling functions have been introduced over more than 60 years (Rostoker et al. 1972; Burton et al. 1975). Of these coupling functions, the Epsilon parameter (Perreault and Akasofu 1978), which strictly follows the condition of IMF orientation, is given by

$$\varepsilon(W) = \frac{4\pi}{\mu_0} \nu B^2 \sin^4(\theta_c/2) l_0^2 \quad (1)$$

where  $\nu$  is the solar wind bulk speed,  $B$  is the strength of interplanetary magnetic field, the parameter  $l_0$  is the empirically determined scale length, which is related to the size of the magnetosphere, and  $\theta_c$  is the IMF clock angle. In the present study, the Epsilon parameters are directly taken from SuperMAG network (<http://supermag.jhuapl.edu/>).

Since ionospheric dissipation and ground magnetic perturbation are two manifestations of a single substorm in the earth's environment, they are highly correlated with each other. The selected substorms are more prominent in the midnight/post-midnight sector than in other sectors of the auroral oval region as they generated well-developed negative bays in magnetic disturbances and associated Pi2s in the same sectors (see Sect. 3.1). Hence, energetic electrons are likely to precipitate more in the midnight/post-midnight sector. Ionospheric Joule heating generated as a result of collision between the energetic electrons and neutrals will therefore also maximise in the same sectors. Moreover, sharp decreases in the IL index, associated with negative bays in the H-component of magnetic disturbances, in the midnight or post-midnight sectors emphasise the presence of magnetic features of substorms in the same sectors. Hence,

ionospheric dissipation through Joule heating, during intense substorms, can be estimated using empirical formulations, connecting ionospheric Joule heating power and local IL index. For the estimation of ionospheric Joule heating during geomagnetically disturbed periods, Tenfjord and Østgaard (2013) have made some adjustment in the empirical formulation of the rate of ionospheric Joule heating using AE index as a proxy (Østgaard et al. 2002). They have modified the empirical relation as a function of the SuperMAG electrojet (SME) index instead of AE, using the ratio of SME to AE as a suitable scaling factor. Reasonable values for solstice Joule heating are thus estimated. Since the IMAGE magnetometer network contains the standard AL station (Abisko) in the midnight sector of auroral oval region, it is unnecessary to put an additional scaling factor in the Ahn's empirical relation connecting Joule heating and the AL index. Based on these, we assume a modified form of the Ahn et al. (1983) relation using the IL index for the estimation of ionospheric Joule heating, localised in the midnight or post-midnight sectors. In other words, energy dissipated through Ionospheric Joule heating, in meridional region of midnight or post-midnight sectors, is estimated using the modified form of the Ahn et al. (1983) empirical conversion formula:

$$\text{Local Joule heating } (W) = 3 \times 10^8 IL \text{ (nT)} \quad (2)$$

A comprehensive view of the Magnetosphere–Ionosphere (MI) system requires large-scale global models of Earth's space environment, along with satellite observations to provide model input. The global models serve as effective tools to determine physical processes in the MI system. Open Geospace General Circulation Model (OpenGGCM) (Raeder et al. 2001) solves the resistive MHD equations, suitable for describing the outer magnetosphere, using spatial differencing schemes and predictor correction schemes. Specifically, it solves the MHD equations in the outer magnetosphere using fourth-order spatial differencing scheme with a minimal diffusion error. Especially, it preserves the condition  $\nabla \cdot B = 0$  by using a specially designed staggered grid method (Evans and Hawley 1988). With the help of a static dipole model, it can map the Ionospheric Field Aligned Current (FAC) to a distance of  $\sim 3R_E$ , at which the magnetosphere and the ionosphere couple to form a single system. Hence, the model covers the entire high-latitude region. The model uses solar wind and IMF data from the ACE and WIND spacecrafts. Data from Geotail and Cluster are also used when they are upstream of the bow shock. A detailed description of the OpenGGCM model is given by Raeder et al. (2008).

Global models, most probably, fail to observe ionospheric response because of the lack of first-order

equation solver for the ionospheric part. Hence, the global models require complementary dynamic coupling models. OpenGGCM model uses the Coupled Thermosphere-Ionosphere Model (CTIM) as a supporting model. It can solve ion fluid equations from 80 to 10,000 km in the ionosphere. The CTIM uses a spherical grid with latitude and longitude resolutions of  $2^\circ$  and  $18^\circ$ , respectively (Fuller-Rowell et al. 1996).

For the present study, Global ionospheric Joule heating rates for the selected substorms during St. Patrick's Day geomagnetic storm are taken from the OpenGGCM coupled with CTIM model using Community Coordinated Modeling Center (CCMC) Run-on-Request system (<https://ccmc.gsfc.nasa.gov/results/index.php>). Solar wind data from WIND spacecraft in GSE Coordinates has been used to drive the simulation with at least 3.5 million grid points.

### Observations

The first superstorm (a geomagnetic storm with  $Dst < -200$  nT) of solar cycle 24 occurred on St. Patrick's Day on 17 March 2015. The Wind spacecraft recorded an interplanetary shock at 03:59 UT, followed by sudden commencement at 04:45 UT on March 17. The storm had a two step intensification; at first  $Dst$  decreased to  $-80$  nT at 10:00 UT on March 17 due to the CME sheath crossing (Le et al. 2016), and then the storm intensified again at 22:00 UT with  $Dst$  reaching  $-223$  nT on March 17 which was associated with a Magnetic Cloud (MC) (Le et al. 2016). After that, the storm fully recovered to its pre-storm state at 04:30 UT on 21 March 2015. Thus, the St. Patrick's Day geomagnetic storm can be considered as a four day two peaked storm.

Recent articles (Le et al. 2016; Tulasi Ram et al. 2015) have clearly described characteristic features of the superstorm. Using multiple satellite observations, Le et al. (2016) have provided a clear picture of the effect of dayside reconnection during this storm period. Also, they noted that field aligned current intensifies significantly during this period. Tulasi Ram et al. (2015) have discussed its effects on electromagnetic conditions in low-latitude pre-midnight sector. However, magnetospheric substorms associated with this superstorm and their signatures in the Earth's magnetosphere are yet to be discussed. In the present study, the ground manifestations of intense substorms, associated with this

superstorm, are investigated. There are tens of substorms during the entire storm; however, we have selected only five substorms in the 22:00 MLT–06:00 MLT sector, covering midnight and post-midnight sectors, of the auroral region showing associated Pi2s and negative bays in the H-component of magnetograms, derived from the IMAGE magnetometer longitudinal (Fennoscandia) chain. All the selected stations in the IMAGE network are proved to be inside the auroral oval for all the selected substorms based on OVATION-Prime model (Newell et al. 2010) using CCMC Run-on-Request system. The OVATION-Prime model provides statistical distribution of precipitating electron and ion fluxes in an MLT-MLAT bin using electrostatic analyzer data from Defense Meteorological Satellite Program (DMSP) satellites. The simulation results are available through the CCMC Website as run numbers 042518\_IT\_1, 042518\_IT\_2, 042518\_IT\_3, 042518\_IT\_4 and 042918\_IT\_1 prefixed with "Suji\_KJ\_".

Figure 1 shows the variation of components of IMF viz  $B_x$ ,  $B_y$  and  $B_z$ , and  $B_{total}$  in GSM coordinates, the GSE x-component of the solar wind velocity ( $v_x$ ), solar wind proton density ( $N_{sw}$ ) and the temperature of the electron flux along the IMF direction, observed by the WIND Spacecraft located at  $\sim 254R_E$  on the Sun–Earth line (L1 point), auroral electrojet indices such as AE and AL indices, local electrojet index (IL) derived from magnetic disturbances observed in the IMAGE magnetometer network, Wp index derived from magnetic disturbances observed in low-latitude magnetometer stations and the  $Dst$  index, during 19:00–05:00 UT on 17–21 March 2015. The selected substorms are numbered as 1, 2, 3, 4 and 5, and durations of their expansion phase are marked with vertical dotted lines.

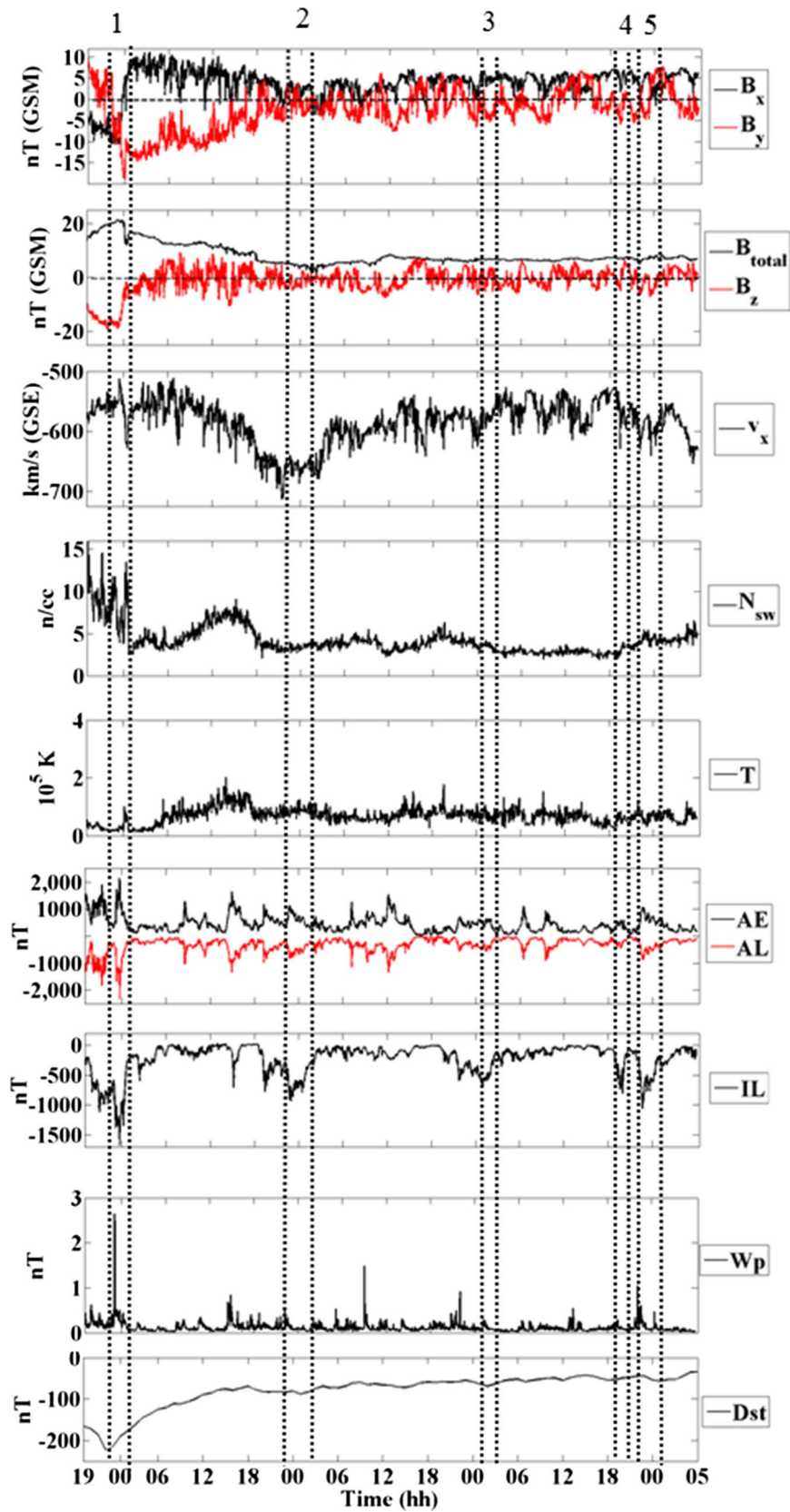
Here, the case study of a substorm that began in the main phase and extended to the recovery phase of the superstorm is presented as a representative of the set.

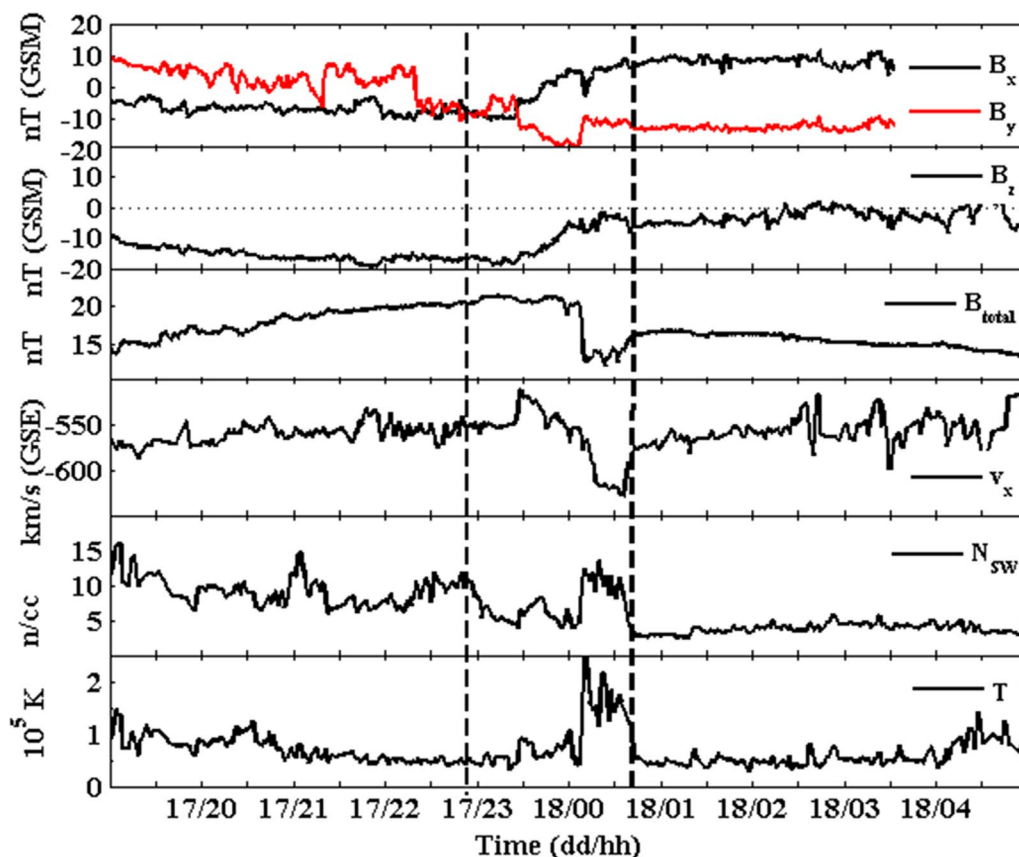
### The event March 17–18, 2015

Figure 2 depicts the IMF and solar wind conditions observed by the WIND Spacecraft located at  $\sim 254R_E$  on the Sun–Earth line (L1 point) during 19:00–05:00 UT on 17–18 March 2015. For comparison, interplanetary magnetic field (IMF) observations and solar wind observations were shifted by  $\sim 46$  min from the WIND position ( $X_{GSE} = \sim 254R_E$ ) to the nose of the Earth's bow shock ( $X_{GSE} = \sim 12R_E$ ). The first three panels show components

(See figure on next page.)

**Fig. 1** From top to bottom: components of IMF viz  $B_x$ ,  $B_y$  and  $B_z$ ,  $B_{total}$ , x-component of solar wind velocity ( $v_x$ ), solar wind density ( $N_{sw}$ ), temperature variation of electron flux along the IMF direction (T), as observed by WIND spacecraft, AE index, AL index, IL index, Wp index and  $Dst$  index, during 19:00–05:00 UT on 17–21 March 2015. Components of interplanetary magnetic field are plotted in GSM coordinates and the x-component of solar wind velocity is plotted in GSE coordinates. The expansion phases of five substorms associated with St. Patrick's Day 2015 geomagnetic storm are marked with vertical dotted lines and substorm numbers are marked at the top





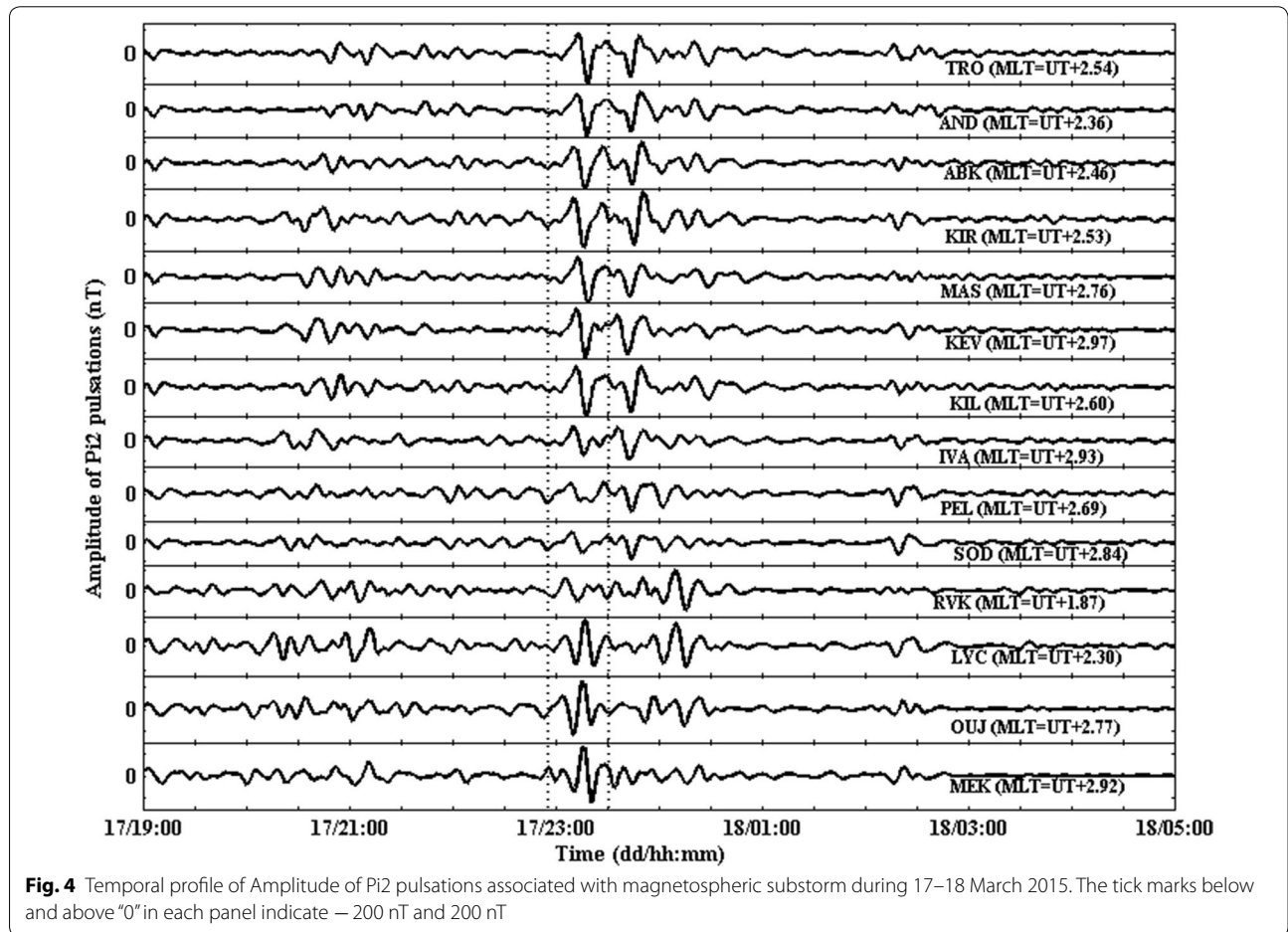
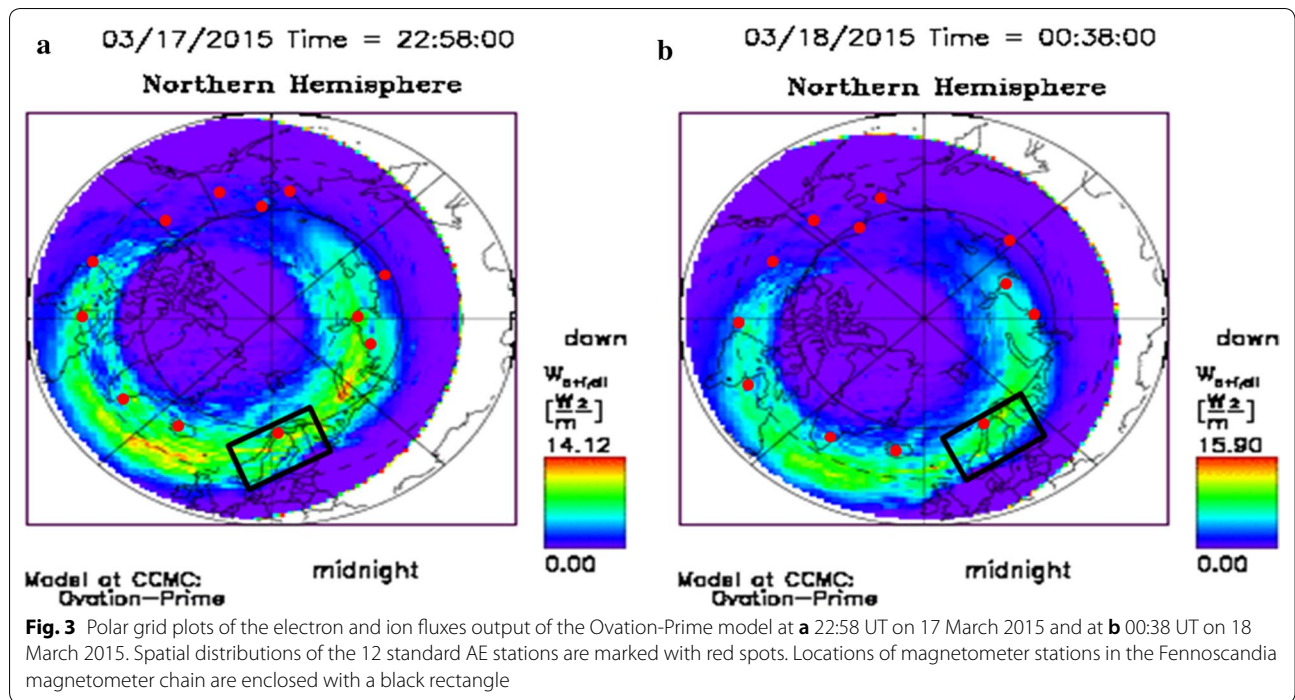
**Fig. 2** From top to bottom: components of IMF viz  $B_x$ ,  $B_y$  and  $B_z$ ,  $B_{total}$ , x-component of solar wind velocity ( $v_x$ ), solar wind density ( $N_{sw}$ ), temperature variation of electron flux along the IMF direction ( $T$ ), as observed by WIND spacecraft during 19:00–05:00 UT on 17–18 March 2015. Components of interplanetary magnetic field are plotted in GSM coordinates and the x-component of solar wind velocity is plotted in GSE coordinates. The expansion phase of the substorm, 17–18 March 2015, during 22:58–00:41 UT on 17–18 March 2015 is marked with two vertical lines

of IMF viz  $B_x$ ,  $B_y$  and  $B_z$ , and  $B_{total}$  in GSM coordinates. The next three panels show the GSE x-component of the solar wind velocity ( $v_x$ ), solar wind density ( $N_{sw}$ ) and the temperature of the electron flux along the IMF direction. The expansion phase of the substorm is marked with two vertical lines. This substorm occurred in the main phase of the superstorm just before the main intensification of the ring current. At 19:00 UT on March 17, IMF  $B_z$  fell to  $-20$  nT and remained approximately constant until 01:30 UT on March 18. The prolonged southward interplanetary magnetic field (IMF  $B_z$ ) persists over a period of 6 h, resulting in large-scale magnetic reconnection (Dungey 1961). Magnetic flux is transported and recombines via nightside reconnection in the magnetotail, causing erosion of the dayside magnetopause (Aubry et al. 1970). During this time, the solar wind velocity peaks at 650 km/s.

Development of substorm episodes leads to transient geomagnetic micro-pulsations (40–150 s) (Saito 1969; Pashin et al. 1982; McPherron et al. 1973). To investigate

latitudinal footprint of these impulses, the closely spaced IMAGE magnetometer chain, located around the auroral oval, has been used. All the stations are confirmed to be inside the auroral oval during substorms, based on precipitating electron and ion fluxes outputs, from Ovation-Prime model (Newell et al. 2010). Figure 3 shows the polar grid plots of the electron and ion fluxes output of the Ovation-Prime model at (a) 22:58 UT on 17 March 2015 and at (b) 00:38 UT on 18 March 2015. Spatial distributions of the 12 standard AE stations are marked with red spots and location of magnetometer stations in the Fennoscandia magnetometer chain are enclosed with a black rectangle. It is evident from Fig. 3 that all the selected stations in the Fennoscandia magnetometer chain are well inside the auroral oval region during this substorm period.

Figure 4 shows the H-component of magnetic disturbances in the ULF band (6.5–25 mHz) observed at 14 stations in Fennoscandia magnetometer chain during 19:00 UT on 17 March–05:00 UT on 18 March 2015. A



prominent impulse ( $\sim 200$  nT) associated with a well-developed negative bay in the H-component of magnetic disturbances, occurs between 22:54 UT on 17 March and 01:00 UT on 18 March for each magnetometer station. The variance in the negative bay is the highest [ $1.0 \times 10^5$  (nT) $^2$ ] for the station OIJ (CGM lat.  $60.99^\circ$  and CGM lon.  $106.14^\circ$ ). The Pi2 event corresponds to the maximum variations of H-component that occurred at 01:44 MLT (22:58 UT) in the midnight sector, for the station OIJ (CGM lat.  $60.99^\circ$  and CGM lon.  $106.14^\circ$ ). Two more impulses ( $\sim 100$  nT), at around 20:00 UT on March 17 and 02:30 UT on March 18, can be seen in Fig. 4. These correspond to two negative bays at respective times.

Figure 5 shows the variation of global and local indices during March 17–18, 2015 substorm event. The first two panels show the AL and Wp indices during the 10-h time interval containing Pi2 events. The next two panels show the variations in H-component and the associated Pi2 event at the station OIJ. The AL index falls to  $\sim 2300$  nT at 23:43 UT on 17 March 2015. The decrease in AL index

and simultaneous increase in Wp index ( $\sim 2.64$  nT) confirm the presence of Pi2 pulsations at OIJ (CGM lat.  $60.99^\circ$  and CGM lon.  $106.14^\circ$ ). The high value of Wp indicates that there should be low-latitude Pi2 events associated with the same substorm event (Nosé et al. 2012). Nosé et al. (2012) have separated the peak values of Wp enhancements into three divisions: A— $\geq 0.4$  nT; B— $\geq 0.2$  nT and  $< 0.4$  nT; C— $< 0.2$  nT. The value of Wp associated with this substorm is shown in Fig. 5a. The onset of Pi2 is marked with a vertical dashed line at 22:58 UT (01:44 MLT in OIJ) on 17 March 2015. Other than this, one more significant Pi2 impulse at around 19:51 UT was clearly seen in the time series. This event is accompanied by simultaneous decrease (increase) in AL (Wp) indices. Here, the Wp enhancement is  $\sim 0.62$  nT, which clearly indicates small-scale substorm intensifications, before the actual auroral breakups (Ohtani et al. 1993).

Earlier studies argued that Pi2s play key roles in the determination of the onset of magnetospheric substorms (Jacobs et al. 1964; Rostoker 1968; Saito et al.

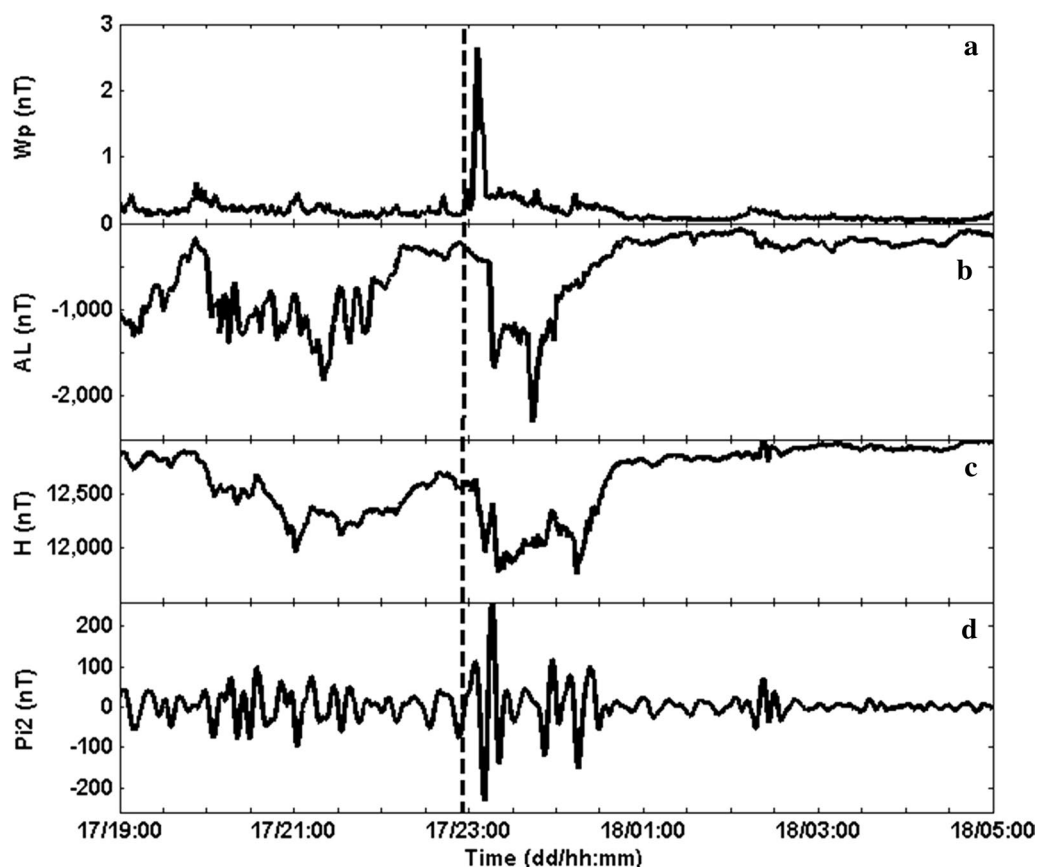


**Fig. 5** Ground signatures of magnetospheric substorm associated with Pi2 pulsations, observed at the station OIJ during 19:00–05:00 UT on 17–18 March 2015. From top to bottom: **a** Wp index, **b** AL index, **c** H-component of magnetic disturbances observed at the station OIJ and **d** associated Pi2 event (filtered in the ULF band of 6.5–25 mHz) at OIJ. The onset of Pi2 is marked with a vertical dashed line at 22:58 UT (01:44 MLT in OIJ) on 17 March 2015



1976; McPherron et al. 1973; Liou et al. 2000). Saito and Sakurai (1970) suggested that auroral substorms, one of the important manifestations of magnetospheric substorms, are frequently associated with Pi2s. Saito and Sakurai (1970) also demonstrated that Pi1, Pc3, and Pc5, and other geomagnetic pulsations occur during substorm expansion phases, while Pi2 pulsations are particularly associated with the onset of substorm expansion. We assume that the onset of a substorm expansion phase can be identified by the occurrence of Pi2 pulsations, up to a temporal difference of the order of seconds (Nosé et al. 1998).

In order to determine the exact time period of expansion phase of an event, we have done a comparative study of local IL index, derived from IMAGE magnetometer network, with IMF  $B_z$ . The variations IMF  $B_z$  and corresponding variations in IL indices for a typical substorm event on 17–18 March 2015 are shown in Fig. 6. The onset of substorm growth phase is marked by the southward turning of the IMF, before the onset of expansion phase (Juusola et al. 2011). The IMF  $B_z$  turns from positive to negative at 19:07 UT, and this is marked as the onset of growth phase. The growth phase continued up to the onset of expansion phase, determined from the commencement of associated Pi2s. We take the end of

the expansion phase to be the time at which the IL index recovers to 1/5 of its minimum value. The duration of expansion phase is limited to about 1 h and 43 min. For the entire substorm, the IMF remained southward. Hence, the substorm is considered as a “continued input substorm”. Since the substorm during 17–18 March 2015 is in the main phase of the superstorm and is also in the prolonged period of a southward IMF  $B_z$ , the substorm under consideration is extremely complex in nature. Hence, multiple expansion phases or small-scale undulations of substorm intensification are most probable to occur, after the single substorm growth phase. The sudden decreases in IL at ~19:26 UT and at ~20:55 UT are due to spatial localisation in magnetic disturbances, associated with the substorm expansion phase, before evolving into larger scales. However, the enormous decrease in the IL index at 22:58 UT can be marked as the onset of the March 17–18, 2015 substorm. The sudden decrease in IL at ~02:10 UT is due to substorm intensifications in the recovery phase.

Using the same method, as discussed above, four more intense substorms associated with the same superstorm were identified. Their onsets have been determined on the basis of global and local observations such as sudden reduction in AL indices, enhancement in Wp indices,

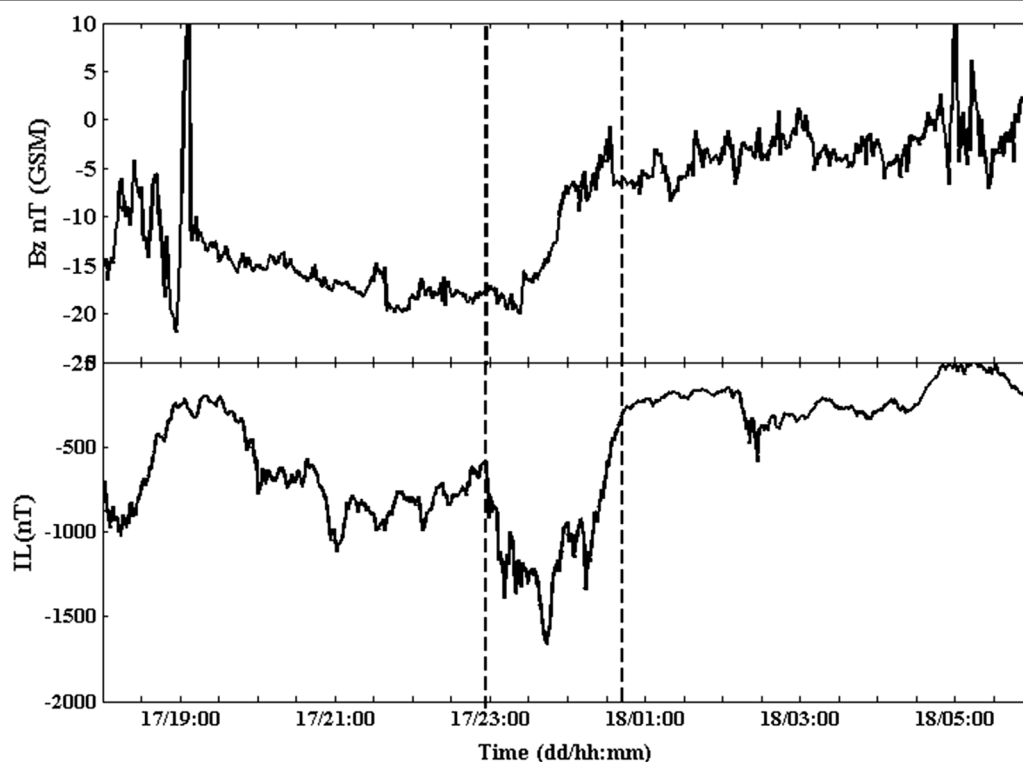


**Fig. 6** Top to bottom: IMF  $B_z$  (in GSM coordinate) from WIND spacecraft and the local electrojet index (IL) derived from the IMAGE magnetometer network, during substorm event 17–18 March 2015. The duration of expansion phase of the substorm is marked with two vertical dashed lines

maximum variance of H-components of geomagnetic disturbances, and onsets of associated Pi2s. Table 2 shows their characteristic features and their time span in MLT.

### Ionospheric Joule heating

In order to estimate the solar wind energy dissipated into inner magnetosphere–ionosphere (MI) system through Joule heating during substorms on 17–18 March 2015, the capabilities of OpenGGCM model and the modified form of Ahn's empirical conversion relation based on the IL index have been applied.

The global auroral electrojet index AL and local auroral electrojet index IL do not follow the same behaviour, over auroral oval region, during geomagnetically disturbed periods. Kauristie et al. (1996) has studied the variation in intensity of global as well as local indices in different MLT sectors by comparing strength of magnetic activity reflected in the AL index with that inferred from the local index, derived from meridional EISCAT magnetometer cross, during different MLT hours. The conclusion of Kauristie et al. (1996) is that the local chain can record better activity than a global one, during the temporal evolution of magnetospheric substorm. During strong geomagnetic activity, the oval expands to such low latitudes that AL chain cannot follow the real temporal behaviour of the electrojet activity. In such cases, a meridional chain can monitor the local intensification in auroral electrojet, in a better way, than that provided by a single AL station. Moreover, the strength of westward electrojet formed

even between two AL stations can also be detected by the IL index (Guo et al. 2014).

During intense storm-time substorms, the auroral oval may move to lower latitudes. The poleward boundary of the oval has the possibility to move to around 65°. On such conditions, AL stations may not be inside the expanding auroral oval and hence, they may not observe the exact features of substorms. For example, it is evident from Fig. 3 that 5 out of the 12 AE stations (viz, YKC, CMO, BRW, CWE and TIK) are located outside the auroral oval boundaries that defined by the OVATION-Prime model during the period of the substorm on 17–18 March 2015. This produces discrepancy for considering the AL index as a global proxy for determining magnetic disturbances, especially during intense storm-time substorms. Meanwhile, the IL index, localised around the midnight or post-midnight MLT sectors, provides the true features of these substorms.

Figure 7a shows the variation of the rate of solar wind impinging the Earth's magnetosphere and that of ionospheric Joule heating, during the period of the substorm on 17–18 March 2015. The duration of the expansion phase has been marked with two vertical dotted lines. The top panel depicts the solar wind energy rate, estimated from the Epsilon parameter (in GW) over a 10-h time interval containing significant Pi2s. At 19:07 UT when IMF  $B_z$  turns southward (Fig. 6), the solar wind energy rate is around 2000 GW. After that, solar wind exhibits variations similar to those of the IMF  $B_z$ . When IMF  $B_z$  reaches its maximum of  $\sim -20$  nT, correspondingly the

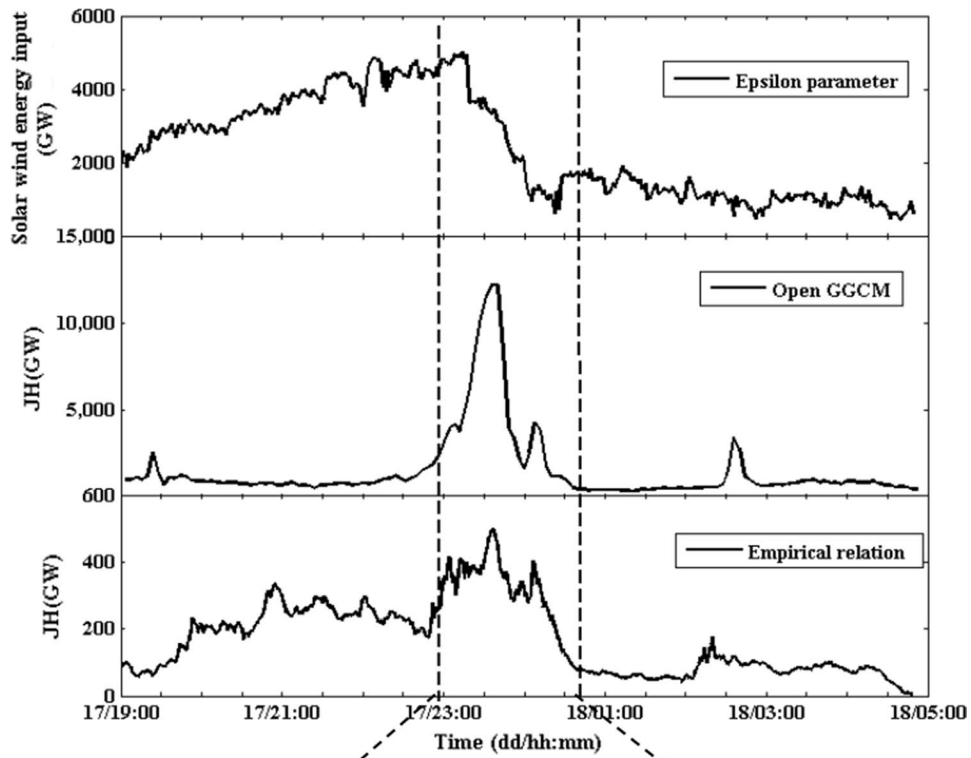
**Table 2** List of substorms in the St. Patrick's Day 2015 geomagnetic storm and the duration of their expansion phases have been derived from ground magnetic perturbations reflected in AL index, Wp index, IL index and H-component of geomagnetic disturbances

Event no	Event list	AL (minimum) (nT)	Wp index (maximum) (nT)	IL index (minimum) (nT)	Variance of H-comp $\times 10^4$ (nT) <sup>2</sup>	Expansion-phase onset (UT)	End of expansion phase (UT)
1	March 17–18	–2300	2.64	–1662	10.08	22:58 (01:44 MLT)	00:41 (03:27 MLT)
2	March 18–19	–841	0.34	–879	4.83	22:28 (00:49 MLT)	01:54 (04:15 MLT)
3	March 20	–551	0.3	–673	3.37	00:18 (02:59 MLT)	02:40 (05:21 MLT)
4	March 20	–440	0.29	–804	3.85	19:16 (22:13 MLT)	20:21 (23:19 MLT)
5	March 20–21	–884	1.0	–1049	6.07	22:05 (00:37 MLT)	00:30 (03:02 MLT)

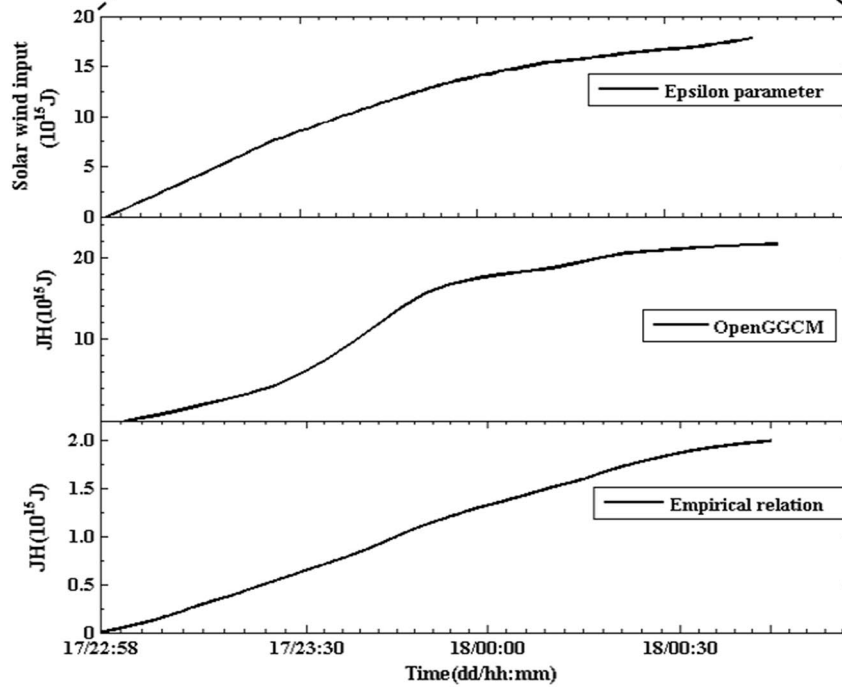
Their time span in MLT is given within brackets

(See figure on next page.)

**Fig. 7 a** From top to bottom: the rate of solar wind energy input estimated from the Epsilon parameter, the rate of global ionospheric Joule heating in the northern hemisphere taken from the OpenGGCM model, and the rate of local ionospheric Joule heating in the midnight sector of the auroral oval region, derived from modified form of the empirical relation based on the IL index, for a typical substorm event, 17–18 March 2015. **b** From top to bottom: the temporal variation of solar wind energy input, global ionospheric Joule heating in the northern hemisphere, estimated from the OpenGGCM model and the local ionospheric Joule heating estimated from the empirical relation based on the IL index, during expansion phase of the substorm event on 17–18 March 2015



a



b

solar wind energy rate reaches its maximum of 4953 GW. At the end of the expansion phase, the solar wind comes down to its pre-substorm value. The second panel of Fig. 7a represents global ionosphere Joule heating in the northern hemisphere (global JH), from the OpenGGCM model. Interestingly, when the expansion phase began the global JH dramatically increased to  $1.22 \times 10^4$  GW which is substantially larger than that in growth or recovery phases of the substorm. Enhancement in the global JH is attributed to the effects of IMF  $B_z$ . When IMF  $B_z$  is sustained and negative, magnetic reconnection rates at the dayside magnetopause increase (Dungey 1961). In order to achieve equilibrium, more fluxes will have to get transported towards nightside magnetosphere where it piles up and is discharged during the substorm expansion phase. The third panel of Fig. 7a represents the rate of local Joule heating (local JH) derived from modified form of Ahn's empirical conversion relation. Figure 7a shows that the maximum rate of local JH is  $\sim 498$  GW ( $\sim 4.1\%$  of the global JH, derived from the OpenGGCM model). The small contribution in the local JH to the global JH indicates that its effect is weak in the post-midnight sector, in this case, corresponding to the northern Scandinavian region. If we instead use the AL index in Ahn's empirical formula, the maximum rate of Joule heating during the substorm is 690 GW ( $\sim 5.6\%$  of the global JH, derived from the OpenGGCM model).

To further examine the variation in ionosphere Joule heating, derived from both the model-based and ground-based methods, time-integrated energies have been determined. Figure 7b shows the temporal variation of the solar wind and simultaneous variations in global as well as local Joule heating, during the substorm event on 19:07 UT on 17 March to 00:41 UT on 18 March 2015. Figure 7b is the portion of the interval between the two dashed lines in Fig. 7a. To determine their relative contributions, the time-integrated solar wind energy inputs from growth phase and expansion phase were examined separately. The substorm event on 19:07 UT on 17 March to 00:41 UT on 18 March 2015 began with a southward turning of the IMF at 19:07 UT far before the onset of the expansion phase. The time-integrated solar wind input energy from 19:07 UT to 22:58 UT on March 17 (corresponding to the growth phase), is estimated to be  $50 \times 10^{15}$  J and that from 22:58 UT on March 17 to 00:41 UT on March 18 (corresponding to the expansion phase) is estimated to be  $18 \times 10^{15}$  J. The solar wind energy input for the entire period of the substorm, hence, is  $69 \times 10^{15}$  J. The energy consumed by global JH is estimated to be  $\sim 22 \times 10^{15}$  J; i.e., 44% of solar wind energy gets dissipated through global JH. The energy consumed by the local JH in meridional region covering post-midnight sector is estimated to be  $2.0 \times 10^{15}$  J (3% of the solar wind input or

9% of the global JH). If we instead use the AL index in the estimation of JH, then the estimate is  $1.7 \times 10^{15}$  J ( $\sim 85\%$  of the JH observed by the IL index).

In the same manner, we have estimated energy content of the other four substorms listed in Table 2. Table 3 presents time-integrated energy values of solar wind energy dissipated through Joule heating calculated from OpenGGCM model output and that estimated from the modified form of Ahn's empirical relation based on the IL index, for all the selected substorms associated with St. Patrick's Day geomagnetic storm. The values within brackets represent Ionospheric Joule heating estimated using the AL index in the empirical relation of Ahn et al. (1983). From 40 to 86% (39–48%, if the IL index is replaced by the AL index in the empirical conversion relation) of the global JH is consumed as the local JH for the substorms in recovery phase of the superstorm.

## Discussion

Several studies utilise the westward electrojet intensities (AL indices) as a measure of substorm intensification as it is directly linked with ionospheric electrodynamic activities. Kallio et al. (2000) have examined JH power during substorms using the local electrojet (IL) index. The local IL index derived from the IMAGE meridional chain records reasonable estimate of the global AL index in the time sectors of 17:30–20:00 UT and 02:00–04:00 UT. That was based on the result by Kauristie et al. (1996), who proposed that for average level of activity ( $-600 \text{ nT} < \text{IL} < -300 \text{ nT}$ ), the relative error between the local IL index and the global AL index becomes  $\sim 20\%$  during 17:30–20:00 UT and 02:00–04:00 UT. But, within the time sector of 20:00–02:00 UT, the IL index overestimates the AL index. Tanskanen et al. (2002)

**Table 3 Time-integrated energy values of solar wind energy dissipated through Joule heating calculated from OpenGGCM model output and that estimated from the modified form of Ahn's empirical relation based on the IL index, for substorms in St. Patrick's Day 2015 geomagnetic storm**

Event no.	Ionospheric Joule heating	
	(Open GGCM model) $10^{15}$ J	(Empirical relation based on IL index) $10^{15}$ J
1	21.63	2.0 (1.71)
2	3.75	2.2 (1.81)
3	2.18	1.2 (0.91)
4	0.68	0.59 (0.31)
5	3.37	1.34 (1.32)

The values within brackets represent ionospheric Joule heating estimated from Ahn's empirical relation based on the AL index

have estimated ionospheric dissipation during isolated and storm-time substorms using IL index, satisfying the conditions stated in Kauristie et al. (1996). Nevertheless, they also noted the inadequacy of the use of IL index as a proxy for global ionospheric dissipation. In the present study, IL index is treated as a local midnight or post-midnight sectors electrojet index, in a way; different form that in Tanskanen et al. (2002) and Kallio et al. (2000). In our study, IL index has been used to obtain local enhancement in magnetic disturbances during magnetospheric substorms and has not been considered to represent global disturbances during the same period. The IL index shows noticeable depression during the substorm expansion phase. It starts to decrease rapidly at substorm onset which synchronises well with Pi2 impulse onset.

Earlier studies (Perreault and Akasofu 1978; Baumjohann and Kamide 1984; Palmroth et al. 2005) suggested that JH during magnetospheric substorms can be derived using global proxies such as AE or AL indices. But in most cases, the estimation based on AE or AL gave underestimated values of ionospheric Joule heating rate. In the study by Baumjohann and Kamide (1984), they attributed the underestimated results were due to the uneven distribution and poor local coverage of the standard AE or AL stations. The AE or AL stations cannot always reside within the auroral oval during an intense geomagnetic storm period. Intense geomagnetic storms may shift the boundaries of oval towards lower latitudes. If that is the case, AE stations may drop outside the oval region, yielding a poor representation of the actual temporal features of substorms. Hence, local indices derived from magnetic perturbations at local sectors in auroral oval region provide a better estimate of local JH. In the present case, since the selected substorms are in the midnight or post-midnight sectors of the auroral oval region, the local IL index derived from the IMAGE magnetometer network well behaved as a proxy for local Joule heating in the same sectors.

It is also well known that energy stored in Earth's magnetotail is explosively released into the inner magnetosphere during the expansion phase of substorm activities. Using methods of remote sensing, Østgaard et al. (2002) confirm that high-latitude ionospheric Joule heating serves as the major dissipation channel in the MI system. JH derived from the OpenGGCM model and JH derived from the empirical relation based on local IL index, have been compared. For all the selected substorms except for the first one, both the global (in the northern hemisphere) and local estimations are comparable. But for the first case, that is the event that began in the main phase of the super storm, the local JH is only 9% of the global JH. If AL were used instead of IL in the estimation of local JH during substorms, then it would have given a lower value.

Global Joule heating in northern hemisphere (global JH) shows an abrupt maximum at the beginning of recovery phase than during those events well inside the recovery phase. These observations are in good agreement with earlier studies based on MHD simulations (Lu et al. 1998; Knipp et al. 1998; Palmroth et al. 2004a, b, 2005). Intense southward IMF orientation and the flow of high stream of solar wind clearly confirm the maximum dissipation (Dungey 1961).

In the case of substorms in recovery phase, the local model using IL index can obtain 40–86% of the globally estimated results. In order to check low-latitude implications of these substorms activities, we further looked into Wp index. The Wp index indicates the presence of low-latitude Pi2 pulsations generated by resonance cavity-mode oscillations in inner magnetosphere (Nosé et al. 2012). This resonance is mainly due to the compressional component of MHD waves produced in the mid-tail lobes during substorm onsets (Teramoto et al. 2016). Lower values in Wp index indicate less intense signatures of substorms in low latitudes. The percentage contribution of local JH in the global JH and the value of Wp index for the selected substorms show that the substorms in the medium level B are likely found to be localised within the high-latitude region. In short, the present study demonstrated that for spatially localised substorms which are more likely found in prolonged recovery phase of superstorms, most of the energy stored in the magnetotail is dissipated in the region where these substorms are actually localised.

The OpenGGCM model coupled with the CTIM model does not completely reflect the magnetosphere-ionosphere behaviour, because of the implied approximations such as total current closure in ionosphere, exclusion of the physics of plasmasphere and absence of the physics for interpreting nonlinearity of the MI system (Li et al. 2011, Connor et al. 2016). In spite of these, the OpenGGCM-CTIM predicts better estimations for global ionospheric Joule heating. Any approximation in the neutral-ion collisional heating rate in neutral-ion equations in Ionosphere-Thermosphere (IT) model for the IT system, definitely, underestimates the simulation result of ionospheric Joule heating rate (Zhu and Ridley 2016). Recently, Li et al. (2011) have investigated the response of ionospheric Joule heating rate to earthward Poynting flux at an altitude of  $\sim 400$  km in high latitudes during geomagnetically quiet period. They have compared the value of Joule heating, estimated from the simulation results of the OpenGGCM-CTIM model, with the downward Poynting flux calculated from the observations of F15 satellite of the Defense Meteorological Satellite Program (DMSP). The JH rate was shown to be in good agreement with the Poynting flux during non storm conditions. In

similar way, Connor et al. (2016) have confirmed better prediction ability of the OpenGGCM-CTIM model for the estimation of global ionospheric Joule heating rates, during quiet and disturbed geomagnetic conditions. Error estimations based on earthward Poynting flux during the selected substorms require electric field and magnetic field measurements from Low Earth Orbiting (LEO) satellites. Such estimation is beyond the scope of the present study, since electric field measurements from Low Earth Orbiting (LEO) satellites are not very reliable during superstorm periods (Balasis et al. 2012; Knipp et al. 2014). Validation of the predictability of the model for global JH estimation during periods of selected substorms requires extensive further analysis, which can be a significant field for future studies.

Local ionospheric Joule heating around magnetospheric onset MLT sectors of the auroral oval region needs prime attention than estimating the global Joule heating over the entire auroral ionosphere during intense storm-time substorms. Global Joule heating response can have a contribution from the associated storm, in addition to the local Joule heating contributed by the substorm itself. local JH around onset location of storm-time substorms provides proper signature of magnetospheric substorms in the same location. The present study proposes local JH as one of the prominent manifestations of magnetospheric substorm activities in the case of storm-time substorms.

## Conclusion

Global ionospheric Joule heating deduced from OpenGGCM model coupled with CTIM model reveals that global response of Joule heating is immensely high for substorms in the main phase of the superstorm whereas global response of Joule heating for the events occurred in the prolonged recovery phase of the superstorm is considerably small (only 3–17% of the global JH for substorms associated with the storm main phase). At the same time, local JH is 9% of the global JH for substorms associated with the main phase of the superstorm and it varies from 40 to 86% of the global JH for those substorms in the storm recovery phase.

One of the reasonable explanations for distinctly different responses in Joule heating observed during main and recovery phases of the superstorm is as follows. During main phase of the storm, there are several pathways whereby energy may be deposited into the ionosphere (Vichare et al. 2005; Li et al. 2012). Hence, the proportion of global Joule heating associated with substorms during main phase is considerably low. On the contrary, during storm recovery phase, when the system is no longer being strongly externally driven, piled up magnetic flux in the tail is redistributed between dayside and nightside via

substorms (Maltsev et al. 1996). This explains the overall larger proportion of global Joule heating associated with substorms during recovery phase.

In short, the present work demonstrates the significance of local Joule heating in auroral oval region, during magnetospheric substorm activities, especially, for storm-time substorms. However, to establish the statistical significance of the results, extensive further studies are needed and are in progress.

## Authors' contributions

KJ and PR made substantial contribution to study, conception and design of the work. KJ carried out data collection and data analysis. PR participated in the verification of analysis and interpretation of results. KJ took the lead in writing the manuscript. PR helped to draft the manuscript. Both authors read and approved the final manuscript.

## Acknowledgements

We are thankful to Space Physics Data Facility's OMNI Web service for providing solar wind plasma data and interplanetary data from WIND spacecraft, the World Data Center for Geomagnetism, Kyoto Website (<http://wdc.kugi.kyoto-u.ac.jp/>) for providing geomagnetic indices such as AL index and Wp index and SuperMAG network (<http://supermag.jhuapl.edu/>) for providing Epsilon parameter. Ground magnetometer data, including IL index, taken from IMAGE network (<http://space.fmi.fi/image/beta/>) is sincerely acknowledged. Simulation results have been provided by the Community Coordinated Modeling Center (CCMC) at Goddard Space Flight Center through their public Runs on Request System (<http://ccmc.gsfc.nasa.gov>). The OpenGGCM model was developed by Joachim Raeder and Timothy Fuller-Rowell at the Space Science Physics Center, UNH. We also wish to thank the CCMC and the originators of the OpenGGCM model for providing the simulation results. The OVATION-Prime model was developed by Patrick Newell and co-workers at Johns Hopkins Applied Physics Laboratory (JHU-APL). We also wish to thank the CCMC and the originators of the OVATION-Prime model for providing the simulation results. Suji K J acknowledges Joint UGC-CSIR senior research fellowship from the University Grant Commission, New Delhi. Last but not least, we would like to thank the anonymous reviewers and the editor, for providing valuable comments and suggestions, which helped a lot in improving this paper considerably.

## Competing interests

The authors declare that they have no competing interests.

## Availability of data and materials

The datasets supporting the conclusions of this article are included within the article and in the following links: <https://space.fmi.fi/image/www/index.php?#>, [https://space.fmi.fi/image/www/index.php?page=il\\_index](https://space.fmi.fi/image/www/index.php?page=il_index), [https://omniw eb.gsfc.nasa.gov/form/sc\\_merge\\_min1.html](https://omniw eb.gsfc.nasa.gov/form/sc_merge_min1.html), <http://supermag.jhuapl.edu/mag?imf=epsilon%2Cgsm>, <http://wdc.kugi.kyoto-u.ac.jp/wdc/Sec3.html>, [https://ccmc.gsfc.nasa.gov/ungrouped/GM\\_IM/GM\\_IM\\_search.php](https://ccmc.gsfc.nasa.gov/ungrouped/GM_IM/GM_IM_search.php).

## Funding

KJ was supported by Senior Research fellowship, granted by UGC-CSIR, New Delhi, through University of Kerala, Trivandrum, India (SRF-Ac.E.IV/III/8605/SRF/2017 DTD. 24.10.2017). The fellowship is for doing research activities, as per the synopsis submitted.

## Publisher's Note

Springer Nature remains neutral with regard to jurisdictional claims in published maps and institutional affiliations.

Received: 12 February 2018 Accepted: 11 October 2018

Published online: 20 October 2018

## References

- Ahn B-H, Akasofu S-I, Kamide Y (1983) The joule heat production rate and the particle energy injection rate as a function of the geomagnetic indices AE and AL. *J Geophys Res* 88:6275–6287. <https://doi.org/10.1029/JA088iA08p06275>
- Akasofu S-I (1981) Relationships between the AE and Dst indices during geomagnetic storms. *J Geophys Res* 86(1):4820–4822. <https://doi.org/10.1029/JA086iA06p04820>
- Aubry MP, Russell CT, Kivelson MG (1970) Inward motion of the magnetopause before a substorm. *J Geophys Res* 75(34):7018–7031. <https://doi.org/10.1029/JA075i034p07018>
- Balasis G, Daglis IA, Zesta E, Papadimitriou C, Georgiou M, Haagmans R, Tsinganos K (2012) ULF wave activity during the 2003 Halloween superstorm: multipoint observations from CHAMP, Cluster and Geotail missions. *Ann Geophys* 30:1751–1768. <https://doi.org/10.5194/angeo-30-1751-2012>
- Baumjohann W, Kamide Y (1984) Hemispherical Joule heating and the AE indices. *J Geophys Res* 89(A1):383–388. <https://doi.org/10.1029/JA089iA01p00383>
- Behera JK, Sinha AK, Vichare G, Bhaskar AT, Honary F, Rawat R, Singh R (2017) Enhancement and modulation of cosmic noise absorption in the afternoon sector at subauroral location ( $L = 5$ ) during the recovery phase of 17 March 2015 geomagnetic storm. *J Geophys Res Space Phys* 122:1–17. <https://doi.org/10.1002/2017JA024226>
- Brekke A, Rino CL (1978) High-resolution altitude profiles of the auroral zone energy dissipation due to ionospheric currents. *J Geophys Res* 83(A6):2517–2524. <https://doi.org/10.1029/JA083iA06p02517>
- Burton RK, McPherron RL, Russell CT (1975) An empirical relationship between interplanetary conditions and Dst. *J Geophys Res* 80(31):4204–4214. <https://doi.org/10.1029/JA080i031p04204>
- Connor HK, Zesta E, Fedrizzi M, Shi Y, Raeder J, Codrescu MV, Fuller-Rowell TJ (2016) Modeling the ionosphere–thermosphere response to a geomagnetic storm using physics-based magnetospheric energy input: OpenGGCM-CTIM results. *J Space Weather Space Clim* 6:A25. <https://doi.org/10.1051/swsc/2016019>
- Dungey JW (1961) Interplanetary magnetic field and the auroral zones. *Phys Rev Lett* 6(2):47–48. <https://doi.org/10.1103/PhysRevLett.6.47>
- Evans CR, Hawley JF (1988) Simulation of magnetohydrodynamic flows—a constrained transport method. *Astrophys J* 332:659–677. <https://doi.org/10.1086/166684>
- Foster JC, St.-Maurice JP, Abreu VJ (1983) Joule heating at high latitudes. *J Geophys Res Space Phys* 88(A6):4885–4897. <https://doi.org/10.1029/JA088iA06p04885>
- Fuller-Rowell TJ, Rees D, Quegan S, Moffett RJ, Codrescu MV, Millward GH (1996) A coupled thermosphere-ionosphere model (CTIM). In: Schunk RW (ed) In STEP report, Scientific committee on Solar Terrestrial Physics (SCOSTEP). NOAA/NGDC, Boulder, p 217
- Guo J, Pulkkinen TI, Tanskanen EI, Feng X, Emery BA, Liu H, Liu C, Zhong D (2014) Annual variations in westward auroral electrojet and substorm occurrence rate during solar cycle 23. *J Geophys Res Space Phys* 119:2061–2068. <https://doi.org/10.1002/2013JA019742>
- Jacobs JA, Kato Y, Matsushita S, Troitskaya VA (1964) Classification of geomagnetic micropulsations. *J Geophys Res* 69:180–181. <https://doi.org/10.1029/JZ069i001p00180>
- Juusola L, Østgaard N, Tanskanen E, Partamies N, Snekvik K (2011) Earthward plasma sheet flows during substorm phases. *J Geophys Res* 116:A10228. <https://doi.org/10.1029/2011JA016852>
- Kallio EI, Pulkkinen TI, Koskinen HEJ, Viljanen A, Slavin JA, Ogilvie K (2000) Loading-unloading processes in the nightside ionosphere. *Geophys Res Lett* 27(11):1627–1630. <https://doi.org/10.1029/1999GL003694>
- Kauristie K, Pulkkinen TI, Pellinen RJ, Opgenoorth HJ (1996) What can we tell about global auroral-electrojet activity from a single meridional magnetometer chain? *Ann Geophys* 14(11):1177–1185
- Knipp DJ, Emery BA, Engebretson M, Li X, McAllister AH, Mukai T, Kakubun S, Reeves GD, Evans D, Obara T, Pi X, Rosenberg T, Weatherwax A, McHarg MG, Chun F, Mosely K, Codrescu M, Lanzerotti L, Rich FJ, Sharber J, Wilkinson P (1998) An overview of the early November 1993 geomagnetic storm. *J Geophys Res* 103:197–220
- Knipp DJ, Matsuo T, Kilcommons L, Richmond A, Anderson B, Korth H, Redmon R, Mero B, Parrish N (2014) Comparison of magnetic perturbation data from LEO satellite constellations: statistics of DMAP and AMPERE. *Space Weather* 12:2–23. <https://doi.org/10.1002/2013SW000987>
- Kozlovskaya E, Kozlovsky A (2012) Influence of high-latitude geomagnetic pulsations on recordings of broad-band force-balanced seismic sensors. *Geosci Instrum Method Data Syst Discuss* 2:107–148. <https://doi.org/10.5194/gid-2-107-2012>
- Le G, Lühr H, Anderson BJ, Strangeway RJ, Russell CT, Singer H, Slavin JA, Zhang Y, Huang T, Bromund K, Chi PJ, Lu G, Fischer D, Kepko EL, Leinweber HK, Magnes W, Nakamura R, Plaschke F, Rauber J, Stolle C, Torbert RB (2016) Magnetopause erosion during the March 17 2015 magnetic storms: combined field-aligned currents, auroral oval, and magnetopause observations. *Geophys Res Lett* 43:2396–2404. <https://doi.org/10.1002/2016GL068257>
- Li W, Knipp D, Lei J, Raeder J (2011) The relation between dayside local Poynting flux enhancement and cusp reconnection. *J Geophys Res* 116:A08301. <https://doi.org/10.1029/2011JA016566>
- Li H, Wang C, Xu WY, Kan JR (2012) Characteristics of magnetospheric energetics during geomagnetic storms. *J Geophys Res* 117:A04225. <https://doi.org/10.1029/2012JA017584>
- Liou K, Meng C-I, Newell PT, Takahashi K, Ohtani S-I, Lui ATY, Brittnacher M, Parks G (2000) Evaluation of low-latitude Pi2 pulsations as indicators of substorm onset using Polar ultraviolet imagery. *J Geophys Res* 105(A2):2495–2505
- Lu G, Baker DN, McPherron RL, Farrugia CJ, Lummerzheim D, Ruohoniemi JM, Rich FJ, Evans DS, Lepping RP, Brittnacher M, Li X, Greenwald R, Sofko G, Villain J, Lester M, Thayer J, Moretto T, Milling D, Troshichev O, Zaitzev A, Odintsov V, Makarov G, Hayashi K (1998) Global energy deposition during the January 1997 magnetic cloud event. *J Geophys Res* 103(A6):11685–11694. <https://doi.org/10.1029/98JA00897>
- Maltsev YP, Arykov AA, Belova EG, Gvozdevsky BB, Safargaleev VV (1996) Magnetic flux redistribution in the storm time magnetosphere. *J Geophys Res* 101:7697–7704
- McHarg M, Chun F, Knipp D, Lu G, Emery B, Ridley A (2005) High-latitude Joule heating response to IMF inputs. *J Geophys Res* 110:A08309. <https://doi.org/10.1029/2004JA010949>
- McPherron RL, Russell CT, Kivelson MG, Coleman PJ (1973) Substorms in space: the correlation between ground and satellite observations of the magnetic field. *Radio Sci* 8(11):1059–1076. <https://doi.org/10.1029/RS008i011p01059>
- Newell PT, Sotirelis T, Wing S (2010) Seasonal variations in diffuse, monoenergetic, and broadband aurora. *J Geophys Res* 115:A03216. <https://doi.org/10.1029/2009JA014805>
- Nosé M, Iyemori T, Takeda M, Kamei T, Milling DK, Orr D, Singer HJ, Worthington EW, Sumitomo N (1998) Automated detection of Pi2 pulsations using wavelet analysis: 1. Method and an application for substorm monitoring. *Earth Planets Space* 50:773–783. <https://doi.org/10.1186/BF03352169>
- Nosé M, Iyemori T, Wang L, Hitchman A, Matzka J, Feller M, Egdorf S, Gilder S, Kumasaka N, Koga K, Matsumoto H, Koshiishi H, Cifuentes-Nava G, Curto JJ, Segarra A, Çelik C (2012) Wp index: a new substorm index derived from high-resolution geomagnetic field data at low latitude. *Space Weather* 10(8):S08002. <https://doi.org/10.1029/2012SW000785>
- Ohtani S, Anderson BJ, Sibeck DG, Newell PT, Zanetti LJ, Potemra TA, Takahashi K, Lopez RE, Angelopoulos V, Nakamura R, Klumpp DM, Russell CT (1993) A multisatellite study of a pseudo-substorm onset in the near-Earth magnetotail. *J Geophys Res Space Phys* 98:355–367. <https://doi.org/10.1029/93JA01421>
- Østgaard N, Germany G, Stadsnes J, Vondrak RR (2002) Energy analysis of substorms based on remote sensing techniques, solar wind measurements, and geomagnetic indices. *J Geophys Res Space Phys* 107(A9):1233. <https://doi.org/10.1029/2001JA002002>
- Palmroth M, Janhunen P, Pulkkinen TI, Koskinen HEJ (2004a) Ionospheric energy input as a function of solar wind parameters: global MHD simulation results. *Ann Geophys* 22:549–566
- Palmroth M, Pulkkinen TI, Janhunen P, Koskinen HEJ (2004b) Ionospheric power consumption in global MHD simulation predicted from solar wind measurements. *IEEE Trans Plasma Sci* 32:1511–1518
- Palmroth M, Janhunen P, Pulkkinen TI, Aksnes A, Lu G, Østgaard N, Watermann J, Reeves GD, Germany GA (2005) Assessment of ionospheric Joule heating by GUMICS-4 MHD simulation, AMIE, and satellite-based statistics: towards a synthesis. *Ann Geophys* 23:2051–2068. <https://doi.org/10.5194/angeo-23-2051-2005>

- Pashin AB, Raspopov OM, Lakhnin AG, Glassmeier KH, Baumjohann W, Opge-noorth HJ, Pellinen RJ (1982) Pi2 magnetic pulsations, auroral break-ups, and the substorm current wedge: a case study. *J Geophys Res* 87:223–233
- Perreault P, Akasofu S-I (1978) A study of geomagnetic storms. *Geophys J R Astron Soc* 54:547–573. <https://doi.org/10.1111/j.1365-246X.1978.tb05494.x>
- Raeder J, McPherron RL, Frank LA, Kokubun S, Lu G, Mukai T, Paterson WR, Sigwarth JB, Singer HJ, Slavin JA (2001) Global simulation of the geospace environment modeling substorm challenge event. *J Geophys Res* 106:381–395
- Raeder J, Larson D, Li W, Kepko EL, Fuller-Rowell TJ (2008) OpenGGCM simulations for the THEMIS mission. *Space Sci Rev* 141:535–555. <https://doi.org/10.1007/s11214-008-9421-5>
- Richmond AD (1992) Assimilative mapping of ionospheric electrodynamics. *Adv Space Res* 12(6):59–68. [https://doi.org/10.1016/0273-1177\(92\)90040-5](https://doi.org/10.1016/0273-1177(92)90040-5)
- Rostoker G (1968) Macrostructure of geomagnetic bays. *J Geophys Res* 73(13):4217–4229. <https://doi.org/10.1029/JA073i013p04217>
- Rostoker G, Lam HL, Hume WD (1972) Response time of the magnetosphere to the interplanetary electric field. *Can J Phys* 50:544–547
- Saito T (1969) Geomagnetic pulsations. *Space Sci Rev* 10:319–412. <https://doi.org/10.1007/BF00203620>
- Saito T, Sakurai T (1970) Mechanism of geomagnetic Pi2 pulsations in magnetically quiet condition. *Sci Rep Tohoku Univ Ser 5 Geophys* 20:49–70. <http://hdl.handle.net/10097/44700>
- Saito T, Yumoto K, Koyama Y (1976) Magnetic pulsation Pi2 as a sensitive indicator of magnetospheric substorm. *Planet Space Sci* 24(11):1025–1029. [https://doi.org/10.1016/0032-0633\(76\)90120-3](https://doi.org/10.1016/0032-0633(76)90120-3)
- Slinker SP, Fedder JA, Emery BA, Baker KB, Lummerzheim D, Lyon JG, Rich FJ (1999) Comparison of global MHD simulations with AMIE simulations for the events of May 19–20, 1996. *J Geophys Res Space Phys* 104(A12):28379–28395. <https://doi.org/10.1029/1999JA900403>
- Tanskanen EI (2009) A comprehensive high-throughput analysis of substorms observed by IMAGE magnetometer network: years 1993–2003 examined. *J Geophys Res* 114:A05204. <https://doi.org/10.1029/2008JA013682>
- Tanskanen E, Pulkkinen TI, Koskinen HEJ, Slavin JA (2002) Substorm energy budget during low and high solar activity: 1997 and 1999 compared. *J Geophys Res Space Phys* 107(A6):1–11. <https://doi.org/10.1029/2001JA900153>
- Tenford P, Østgaard N (2013) Energy transfer and flow in the solar wind–magnetosphere–ionosphere system: a new coupling function. *J Geophys Res Space Phys* 118:5659–5672. <https://doi.org/10.1002/jgra.50545>
- Teramoto M, Nishitani N, Nishimura Y, Nagatsuma T (2016) Latitudinal dependence on the frequency of Pi2 pulsations near the plasmapause using THEMIS satellites and Asian–Oceanian Super DARN radars. *Earth Planets Space* 68:22. <https://doi.org/10.1186/s40623-016-0397-1>
- Tulasi Ram S, Yokoyama T, Otsuka Y, Shiokawa K, Sripathi S, Veenadhari B, Heelis R, Ajith KK, Gowtam VS, Gurubaran S, Supnithi P, Le Huy M (2015) Dusk-side enhancement of equatorial zonal electric field response to convection electric fields during the St. Patrick's Day storm on 17 March 2015. *J Geophys Res Space Phys* 121:538–548. <https://doi.org/10.1002/2015JA021932>
- Vichare G, Alex S, Lakhina GS (2005) Some characteristics of intense geomagnetic storms and their energy budget. *J Geophys Res* 110:A03204. <https://doi.org/10.1029/2004JA010418>
- Vickrey JF, Vondrak RR, Matthews SJ (1982) Energy deposition by precipitating particles and Joule dissipation in the auroral ionosphere. *J Geophys Res Space Phys* 87(A7):5184–5196. <https://doi.org/10.1029/JA087iA07p05184>
- Xiong C, Lühr H, Wang H, Johnsen MG (2014) Determining the boundaries of the auroral oval from CHAMP field-aligned current signatures-Part 1. *Ann Geophys* 32:609–622. <https://doi.org/10.5194/angeo-32-609-2014>
- Zhu J, Ridley AJ (2016) Investigating the performance of simplified neutral-ion collisional heating rate in a global IT model. *J Geophys Res Space Phys* 121:578–588. <https://doi.org/10.1002/2015JA021637>

**Submit your manuscript to a SpringerOpen® journal and benefit from:**

- Convenient online submission
- Rigorous peer review
- Open access: articles freely available online
- High visibility within the field
- Retaining the copyright to your article

---

Submit your next manuscript at ► [springeropen.com](http://springeropen.com)

---